Cloud Publications
International Journal of Advanced Remote Sensing and GIS
2015, Volume 4, Issue 1, pp. 990-1007, Article ID Tech-375
ISSN 2320 - 0243

Research Article | Open Access

Mapping Land Cover Classes in the Southern State of Rio Grande Do Sul, Brazil, Using Multiple Endmember Spectral Mixture Analysis (MESMA) Model Applied to Hyperion/EO-1 Hyperspectral Data

Rodrigo de Marsillac Linn[1] and Silvia Beatriz Alves Rolim[2]

[1]SMUrb, Secretaria Municipal de Urbanismo, PMPA, Prefeitura Municipal de Porto Alegre, RS. [2]CEPSRM/UFRGS, Centro Estadual De Pesquisas em Sensoriamento Remoto e Meteorologia, Federal University of Rio Grande do Sul State, Brazil

Correspondence should be addressed to Silvia Beatriz Alves Rolim, silvia.rolim@ufrgs.br

Publication Date: 29 April 2015

Article Link: http://technical.cloud-journals.com/index.php/IJARSG/article/view/Tech-375

Abstract In this paper we evaluated the potential use of Multiple Endmember Spectral Mixture Analysis (MESMA) applied to EO-1 Hyperion hyperspectral data to separate land covers (soil = dunes and dry fields; green vegetation = pinus, eucalyptus and grasslands; water = without sediments, with sediments, and with chlorophyll; and shade), in the southern state of Rio Grande do Sul, Brazil. The approach involved (a) preprocessing and atmospheric correction of Hyperion image; (b) sequential use of Minimum Noise Fraction (MNF), Pixel Purity Index (PPI) and n-Dimensional Visualizer techniques in the visible to shortwave range for the initial selection of a group of endmember, and another group of pixels for model validation; (c) use of the software Visualization and Image Processing for Environmental Research (VIPER) Tools to perform the final selection of endmembers based on the spectral library, and to obtain MESMA models; and (d) evaluation of resulting fraction images and RMSE values to determine the optimal number of endmembers of the MESMA model. Results showed that a four-endmember MESMA model described the diversity of the scene components, including that of materials within the same class (e.g., pinus and eucalyptus) and produced the largest fractions and the lowest RMSE values on a per-pixel basis. Results also showed the performance of MESMA applied to Hyperion data to discriminate properly land covers in the coastal plains, even considering the low signal-to-noise ratio of the instrument.

Keywords *Spectral Mixture Analysis; Spectral Classification; Spectral Library; Hyperspectral Data; Image Processing; Signatures*

1. Introduction

The uncontrolled expansion of urban centers and intensive cultivation of rice, pinus and eucalyptus have greatly contributed to the contamination of soil and lagoon bodies of the coastal plain of Rio Grande do Sul, southern Brazil. In order to support the planning and monitoring of these areas, traditional techniques of digital classification (e.g. MaxVer) have been widely used in images obtained by orbital sensors. However, because of the similarity spectrum between some types of targets (e.g. pinus vs. eucalyptus) and low spectral resolution sensors used for these studies, for example, ETM+ (Landsat 7) with eight spectral bands, different targets are not properly broken down, producing qualification and quantification errors.

Besides, the spectral response of a pixel is an integrated sum of the spectral responses of the scene targets registered by the instantaneous field of view (IFOV) of the sensor. As an example, one can cite soil, vegetation, water, shadow of clouds, and atmospheric contributions [4].

To minimize the poor spectral resolution limitation, it was used the Hyperion sensor, released in November 2000 aboard the Earth Observing-1 satellite (EO-1). With pushbroom scanning mode, the instrument is capable of acquiring orbital images with 242 bands (10 nm of bandwidth) in the visible (VIS), near infrared (NIR) and shortwave infrared (SWIR) (400 – 2500 nm range) with a spatial resolution of 30 m and a swath width of 7.7 km [1]. The sensor allows the extraction of an almost continuous reflectance spectrum for each scene element [2, 3].

In order to identify the ratio of the different materials that comprise a pixel we can decompose the pixel into its pure components or endmembers through spectral mixture models. In this context, there is the Spectral Mixture Analysis (SMA) [5], a digital image-processing tool that can separate the relative ratio of each material within a pixel through the use of a set of pure components. However, According to [12], the SMA fails in that it considers all pixels to be a mixture of a single initial set of endmembers. In this case, there is the chance of a pixel be modeled by endmembers, even if any of these are not present.

As an alternative, we applied the Multiple Endmember Spectral Mixture Analysis (MESMA) [6] model was proposed. The MESMA model enables the number and type of endmembers, and their prevalence, to vary from pixel to pixel, establishing the best-fit mixture model for each pixel individually.

In this paper we evaluate the performance of hyperspectral data (Hyperion orbital sensor) and a Multiple Endmember Spectral Mixture Analysis (MESMA) model to discriminate land cover classes in the coastal plains of Rio Grande do Sul.

2. Materials and Methods

2.1. Study Area

The study area is part of the coastal plain in northeast Rio Grande do Sul, Brazil, between 29°46'28.04"S / 50°15'4.57"W and 30°1'55.75"S / 50°10'18.02”W (Figure 1), in a rectangular area of 7.68 by 27 km. An ASTER image, Level 1B was used to test and perform the techniques.

The topography of the region (20 m of altitude) is flat and lagoon bodies prevail (Figure 2). The climate is subtropical with a mean temperature of 20°C. The annual rainfall varies between 1000 and 1500 mm.

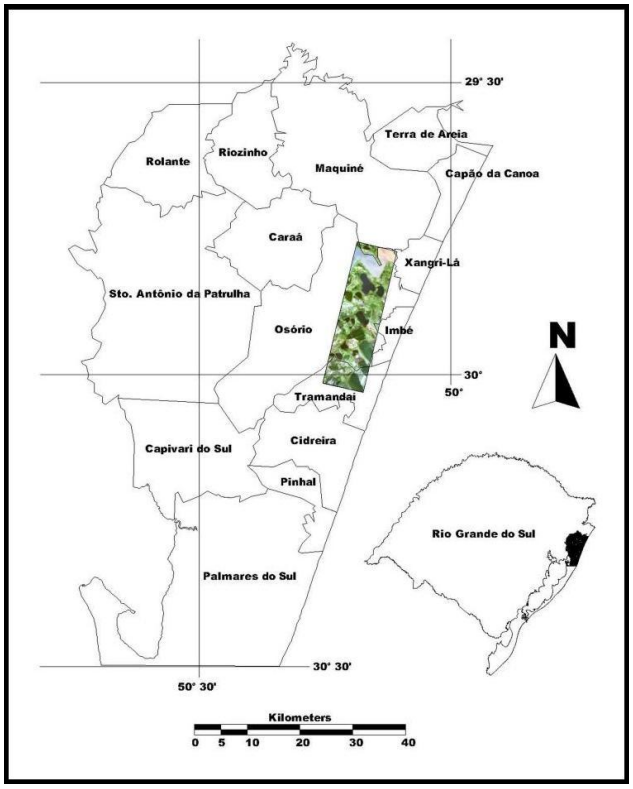

Figure 1: *Study Area*

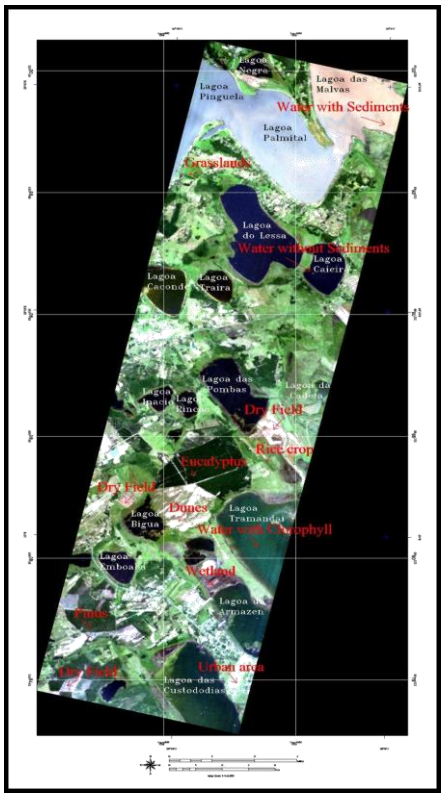

Figure 2: *True Color Composition with Bands Placed at 638 nm (Red), 546 nm (Green) and 465 nm (Blue). The Major Components of the Scene have been identified*

The land use is dominated by small urban centers (e.g. Osório, Tramandaí, Cidreira), rice cultivation (Figure 3 (d)) and pinus (Pinus elliottii) (Figure 3 (e)) and eucalyptus (Eucalyptus sp.) plantations (Figure 3 (a)) in small and medium farms. As for land cover, open fields composed of creeping vegetation, especially grasses (Panicum reptans and Spartina) prevail. These grasses, interspersed with shrubs, are also present in the dunes of quartz sand (Figure 3 (f)). Dry fields, characterized by sparse dry vegetation, are composed of dry pinus branches and rice straw, as shown in Figures 3 (c) and 3 (b).

Figure 3: *Major Components of the Scene Identified in the Area of Study: (a) Eucalyptus, (b, c) Dry Field, (d) Rice, (e) Pinus, and (f) Dunes*

2.2. Image Acquisition and Preprocessing

This study used an EO-1 Hyperion stock image, level L1R (USGS), acquired on May 2nd, 2004, covering part of the coastal plain of Rio Grande do Sul.

According to [12], *the stages of the preprocessing of Hyperion data involved: correction of anomalous pixels (stripes) by interpolation; exclusion of bands with no data of the L1R product and positioned around the atmospheric absorption bands (1,400 nm and 1,900 nm); conversion of data into surface reflectance values by using a radiative transfer model based on MODTRAN-4; and georeferencing image (nearest-neighbor resampling)*.

2.3. Endmember Selection and Spectral Unmixing

The Minimum Noise Fraction (MNF), Pixel Purity Index (PPI) and n-Dimensional Viewer processing sequence was applied to the 143 bands selected from the 454 - 2334 nm interval in order to produce a spectral library and generate a group of samples to validate results obtained by MESMA.

To select endmembers, the PPI image was superimposed on the reflectance image. This overlap also identified the components of the scene that would be represented in the mix model. Thereafter, for each group, pixels identified as "pure" and located in areas where the identification was carried out in the field were grouped into Regions of Interest (ROIs), according to their respective class.

The criteria to select "pure" pixels for the spectral library and for sample validation included: (a) to have been identified by the PPI process, (b) to be located in a homogeneous area, (c) to be from different regions, and (d) to have been verified in the field to which class it belongs.

Three metrics were used in the selection of the most representative spectra of the spectral library: Endmember Average RMSE (EAR) [7], Minimum Average Spectral Angle (MASA) [8] and Count-Based Endmember Selection (CoB) [9], all of them included in the Visualization and Image Processing for Environmental Research (VIPER) Tools software [10]. According to [12], the spectrum obtained the best performance in each metric (the lowest values for EAR and MASA and the highest CoB), were selected to generate the MESMA models. Two, three, and four endmember MESMA models were applied to the Hyperion data [12].

2.4. Accuracy Assessment

The assessment of accuracy was performed in the unmixed pure pixels (validation sample) resulting from the PPI process.

For a model unmix a pure pixel of a given material, in theory it would use a fraction close to 100 % of its corresponding class in the model, regardless the number of endmembers. Thus, for the other endmembers, the fractions would tend to 0%.

In this paper, the fractions produced for each material and models were compared with the RMSE produced in order to evaluate the performance of the MESMA models.

3. Results and Discussion

The PPI process was applied to the first nine MNF bands, which represented a coherent part of the image (devoid of noise), to detect endmember candidate pixels. In total, 14,101 pixels were identified as candidates for endmembers (Figure 4), representing 6.12% of the area imaged.

The pixels identified by the PPI technique occurred mainly in portions of the scene of eight subclasses related to three main classes (water, vegetation and soil): water with sediment (e.g. Lagoa das Malvas), water without sediment (e.g. Lagoa da Caieira), and water with chlorophyll (e.g. Lagoa Tramandaí) (water); pinus, eucalyptus, and grasses (vegetation); and dunes and dry field (soil).

To build the spectral library, 105 pixels were selected as Regions of Interest (ROIs) by subclass (see Table 1), except for the subclass dry field, which had only 20 pixels identified by the PPI process. To compose the validation sample, 80 pixels were selected for each subclass. For the subclass dry field, neighboring pixels identified by the PPI technique were selected to form the spectral library.

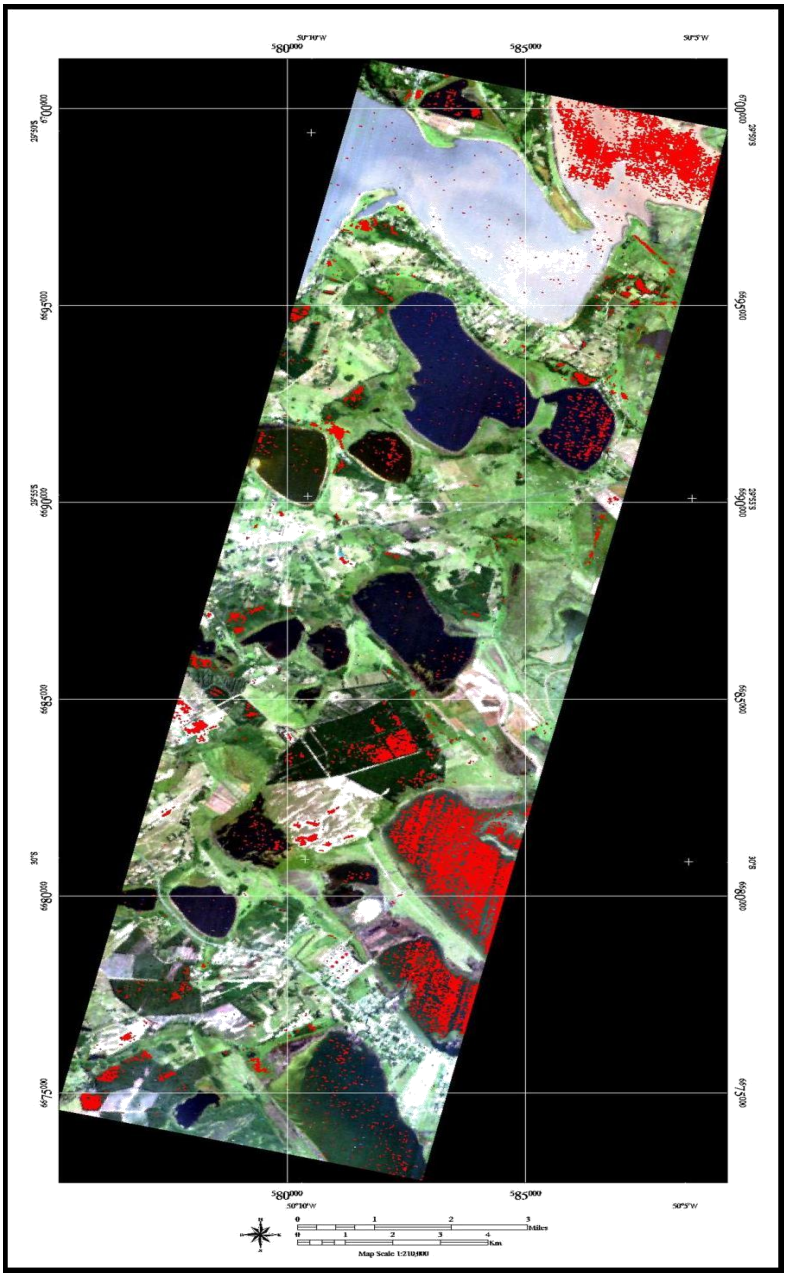

Figure 4: *Pixels in Red (14,101 Pixels) Represent Candidates as Endmembers identified by PPI Technique on the First Nine MNF Bands*

Table 1: *Classes, Subclasses and Number of Pixels Selected to Compose the Spectral Library and the Validation Sample, Resulting from the Sequential Application of MNF and PPI Techniques*

Classes	Subclasses	Number of pixels Spectral Library	Number of pixels Validation Sample
Water	Water with Sediments	105	80
	Water without Sediments	105	80

	Water with Chlorophyll	105	80
	Pinus	105	80
Vegetation	Eucalyptus	105	80
	Grasslands	105	80
Soil	Dunes	105	80
	Dry Fields	20	80
	Total of pixels	755	640

The locations from which the pixels for the eight subclasses were manually extracted are shown in Figure 5.

To calculate metrics fit (RMSE and spectral angle); all 755 spectra from the spectral library were computed. Error values (RMSE), spectral angle, endmember fraction (EM fraction), shade fraction and constraint code were calculated from the spectral unmixing: lines (x axis) for the spectral column (y axis). Results are shown below in five square array images (755 columns X 755 lines), in which the gray levels are associated with the values produced by each metric adjustment.

Figure 6 illustrates the variations associated with Root Mean Square Error (RMSE) in the process of class and subclass spectra modeling. By visually examining Figure 6, one can note that spectra of class water produced the highest RMSE values (lighter pixels/pixels lighter) to model spectra of classes' soil and vegetation. This was due to the difference in brightness between the classes. The lowest RMSE in each class (when spectra of the same class are modeled together) were obtained by the spectra with the highest brightness: water with sediment (water), dunes (soil) and grasses (vegetation). In class water, spectra of water with chlorophyll and water without sediment showed low RMSE when modeled together. The same was true for the class vegetation, where pinus and eucalyptus showed low RMSE, which could result in commission errors.

Variations in the SAM angle (radians) for each class and subclass are shown in Figure 7. As the SAM technique considers only the angle generated between two spectra, it ends up being less influenced by the variation in brightness, apparently producing better results (greater differentiation between the classes). However, just like the RMSE metric adjustment, SAM showed low angles (radians) when spectra of water with chlorophyll and water without sediment, and spectra of pinus and eucalyptus were modeled together.

Figure 8 shows that just as with the RMSE, the values of endmember fraction used by column "x" spectrum to model line "y" spectrum are also related to its brightness value. Spectra with the greatest brightness modeled darker spectra, producing fractions of less than 100%. Moreover, spectra of darker classes modeled spectra of lighter classes, reaching maximum fraction (100%) (e.g. spectra of water with chlorophyll modeling spectra of dunes).

Since x-column spectra modeled y-line spectra by also using the shade endmember, with fraction values of non-shade spectra remaining within the 0-100 % range, shade fractions resulted from the difference of the fraction used by the non-shade spectrum of the column (reference spectra) minus 1.00.

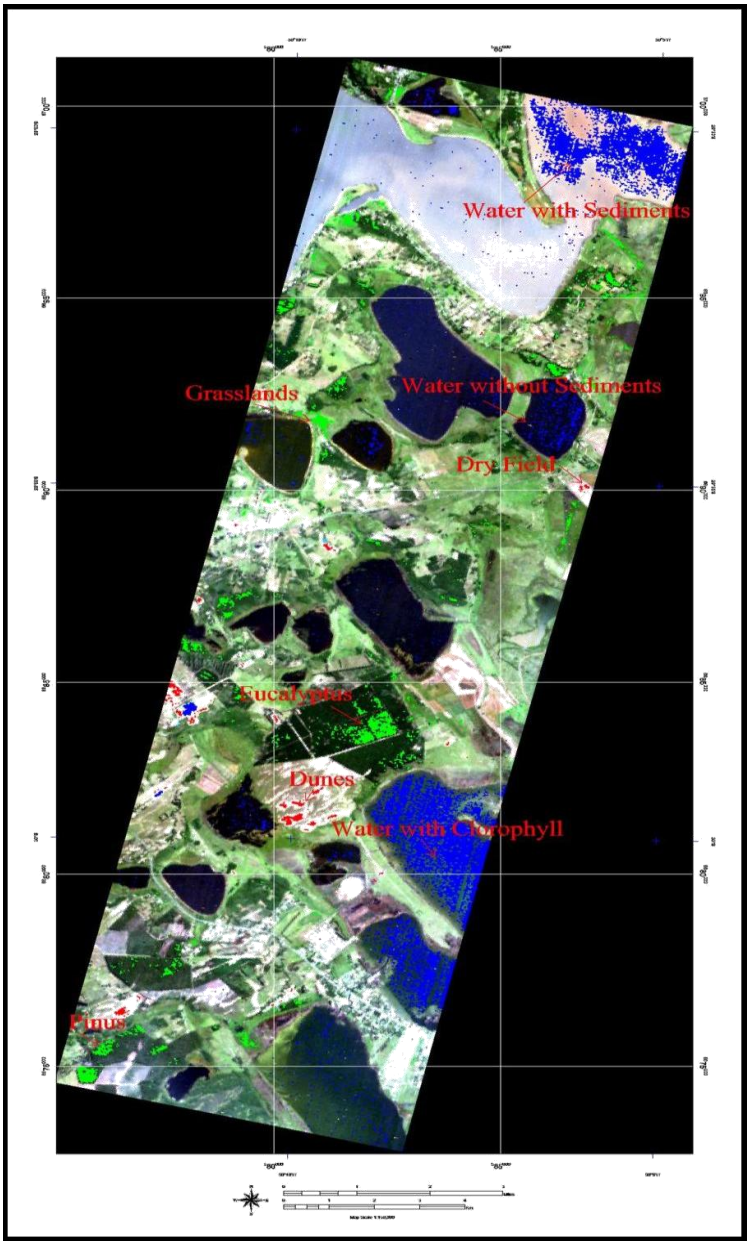

Figure 5: *Parts of the Hyperion Scene, from Which the Pixels Chosen by Sequential Application of MNF and PPI Techniques were extracted to form the Spectral Library and the Validation Sample, Comprising Eight Subclasses of Covers. True Color Combination, with Bands Positioned at 638 nm (Red), 546 nm (Green), and 465 nm (Blue)*

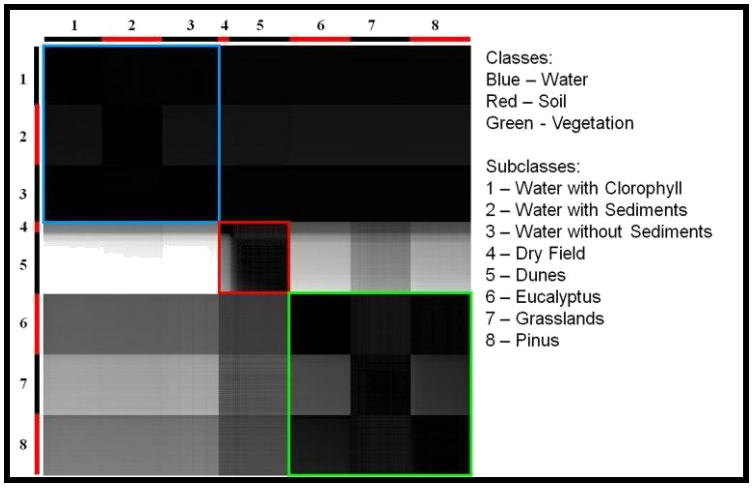

Figure 6: *RMSE Square Array Image – RMS Error Produced By Y-Column Spectrum to Model X-Line Spectrum*

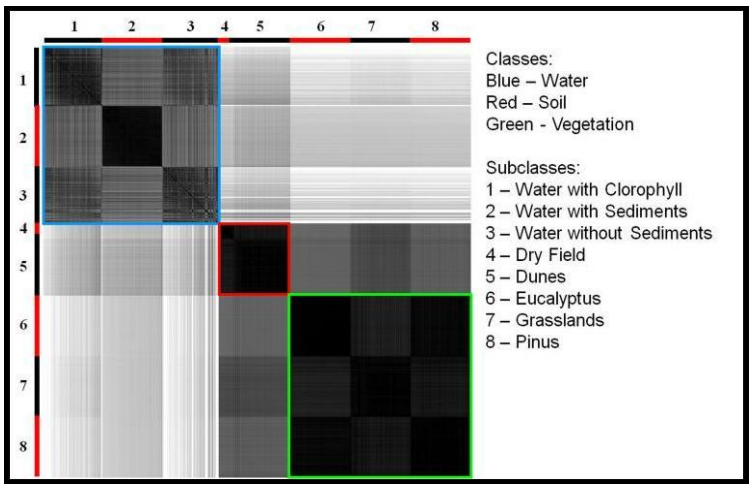

Figure 7: *Square Array Image – SAM – Angle Distance Measured in Radians and Formed Between Column Spectrum (Y Axis; Reference Spectrum) and Line Spectrum (X Axis)*

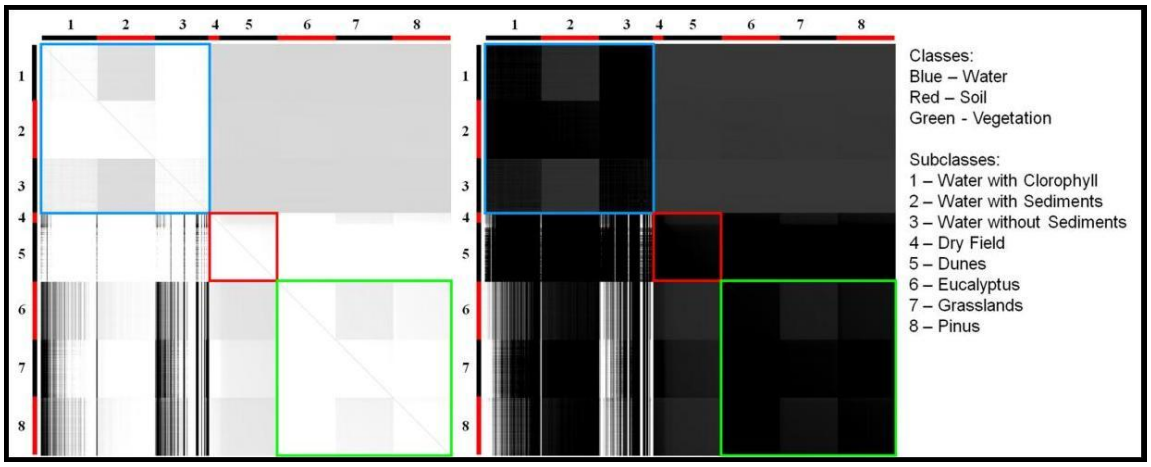

Figure 8: *Square Array Image – Endmember Fraction and Shade Fraction – Corresponds to the SMA Fraction Used by the Column Spectrum (Y Axis) to Model the Line Spectrum (X Axis). Values for the Shade Fraction Were Calculated By the Subtraction of the Spectrum Fraction Minus 1*

For the CoB metric, spectra of the class water did not model other classes (Figure 9). However, spectra of water with chlorophyll and water without sediment were modeled by all other spectra of other classes of the spectral library, without any limitation (Code "0"). The exception was the spectra of water with chlorophyll, which were modeled by the spectra of water without sediment with partial restriction (Code "1" - fraction above 100%, but with a RMSE of less than 0.025). The spectra of water with sediment, dry field, dunes, and grasses were modeled solely by their own spectra (specialist spectra). In the class vegetation, almost all pinus spectra modeled the eucalyptus spectra without any limitation (Code "0"). Some grass spectra modeled pinus spectra, as well as some eucalyptus spectra, with partial restriction. Spectra of the class soil did not model spectra of the class vegetation, and conversely.

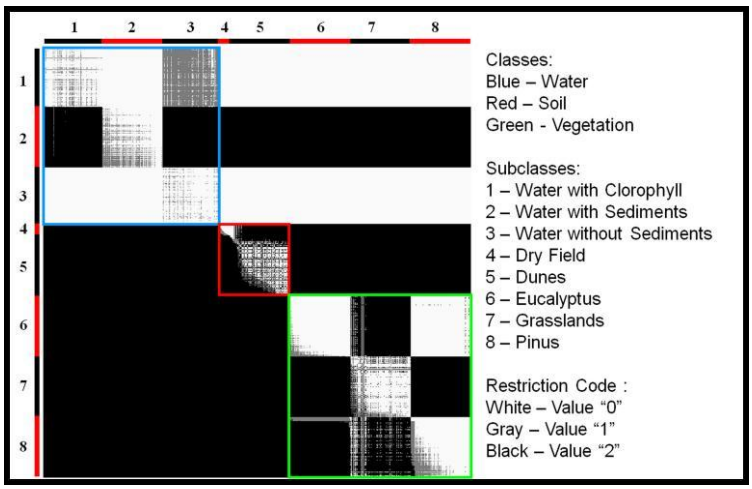

Figure 9: *Constraint Code Image – "1" Indicates Whether the Model was Partially Restricted (Fractions Modeled Exceeded the Limit, but did not Exceed the Specified RMSE), "2" Indicates Whether the RMSE was Exceeded (Completely Restricted), and "0" (Zero) Indicates Models without Any Restriction*

We reached the conclusion that due to the spectral similarity between materials of the same class there might be some confusion when these spectra are associated with a single component of the mixed model. This was clearly observed between the subclasses water with chlorophyll and water with sediment, and between pinus and eucalyptus. Thus, the analysis of square array images allows the user to predict where potential errors of commission might occur.

3.1. Endmember Selection

The application of the metric EAR, MASA and CoB resulted in the selection of 23 representative spectra of the eight subclasses mentioned previously (see Table 2). For the subclass dunes, spectra were selected by only using EAR and MASA metrics, because CoB showed a very low or discrepant value.

As Table 2 illustrates, spectra that showed the lowest EAR also had the lowest MASA. In these cases, spectra with the second lowest MASA were chosen.

Reflectance spectra of Hyperion image pixels shown in Table 2 are shown in Figure 10. Spectra representing the class water had very dissimilar behaviors. Spectra of the subclass water with sediment showed peak reflectance (ρ = 11.3%) in the red range (618 nm), typical of water with high concentrations of suspended inorganic materials. Water with chlorophyll showed the highest reflectance (ρ = 3.74%) in the green range (567 nm), which is a strong indicator of the presence of suspended organic matter. Water without sediment showed the lowest reflectance values, approximately 1.88% for the entire region of the visible, indicating absence of suspended matter.

Table 2: *Pixels Selected (23 Endmember Candidates) by EAR, MASA and CoB (EMC) Metrics to Compose the Second Spectral Library*

No	Endmember	Class	EAR	MASA	CoB
1	DryField_X252_Y313	Soil	0,004189	0,01828	0
2	DryField_X250_Y313	Soil	0,005129	0,018854	0
3	DryField_X253_Y314	Soil	0,005789	0,026221	0,004726
4	Dunes_X117_Y639	Soil	0,02091	0,049839	0
5	Dunes_X112_Y646	Soil	0,023756	0,048694	0
6	Eucalyptus_X161_Y556	Vegetation	0,002973	0,017533	0
7	Eucalyptus_X163_Y555	Vegetation	0,003024	0,017624	0
8	Eucalyptus_X158_Y551	Vegetation	0,004856	0,028736	0,004928
9	Grasslands_X52_Y305	Vegetation	0,010109	0,034415	0
10	Grasslands_X52_Y307	Vegetation	0,010208	0,034936	0
11	Grasslands_X58_Y308	Vegetation	0,010714	0,036702	0,004693
12	Pinus_X21_Y888	Vegetation	0,00507	0,023631	0,003237
13	Pinus_X18_Y893	Vegetation	0,005328	0,0241	0
14	Pinus_X25_Y889	Vegetation	0,005253	0,024516	0,003237
15	Water with Clorophyll_X180_Y615	Water	0,00254	0,231465	0
16	Water with Clorophyll_X207_Y722	Water	0,002558	0,233612	0
17	Water with Clorophyll_X225_Y756	Water	0,004374	0,41362	0,010105
18	Water with Sediments_X144_Y15	Water	0,003029	0,075188	0
19	Water with Sediments_X209_Y25	Water	0,003369	0,077079	0
20	Water with Sediments_X142_Y13	Water	0,01568	0,412722	0,004928
	Water without				
21	Sediments_X171_Y253	Water	0,002487	0,333666	0
	Water without				
22	Sediments_X203_Y239	Water	0,002498	0,334485	0
	Water without				
23	Sediments_X171_Y258	Water	0,002727	0,369349	0,989796

Spectra selected to represent the three subclasses of vegetation showed typical spectral curves of healthy green vegetation, characterized by high absorption of electromagnetic radiation in the regions of blue and red, and high reflectance in the near infrared region beyond the absorption features in the 0.98 and 1.2 μm wavelengths caused by the presence of leaf water.

Pinus and eucalyptus reflectance values showed small differences in the near infrared, between 41% and 36% respectively, and a very similar spectral curve. Some spectra of these tree species that were not selected, but which belonged to the spectral library, had intermediate reflectance values for both species.

Grass spectra reached that same wavelength, i.e. 51 % of reflectance. Spectra of class soil also behaved very typically, with increasing reflectance values related to the increase in wavelength.

Spectra of sand dunes, composed of quartz sand, had a high reflectance at all wavelengths, the main characteristic of the mineral quartz. On the other hand, dry field spectra showed lower reflectance, with peak

(ρ = 33 %) at 1295 nm.

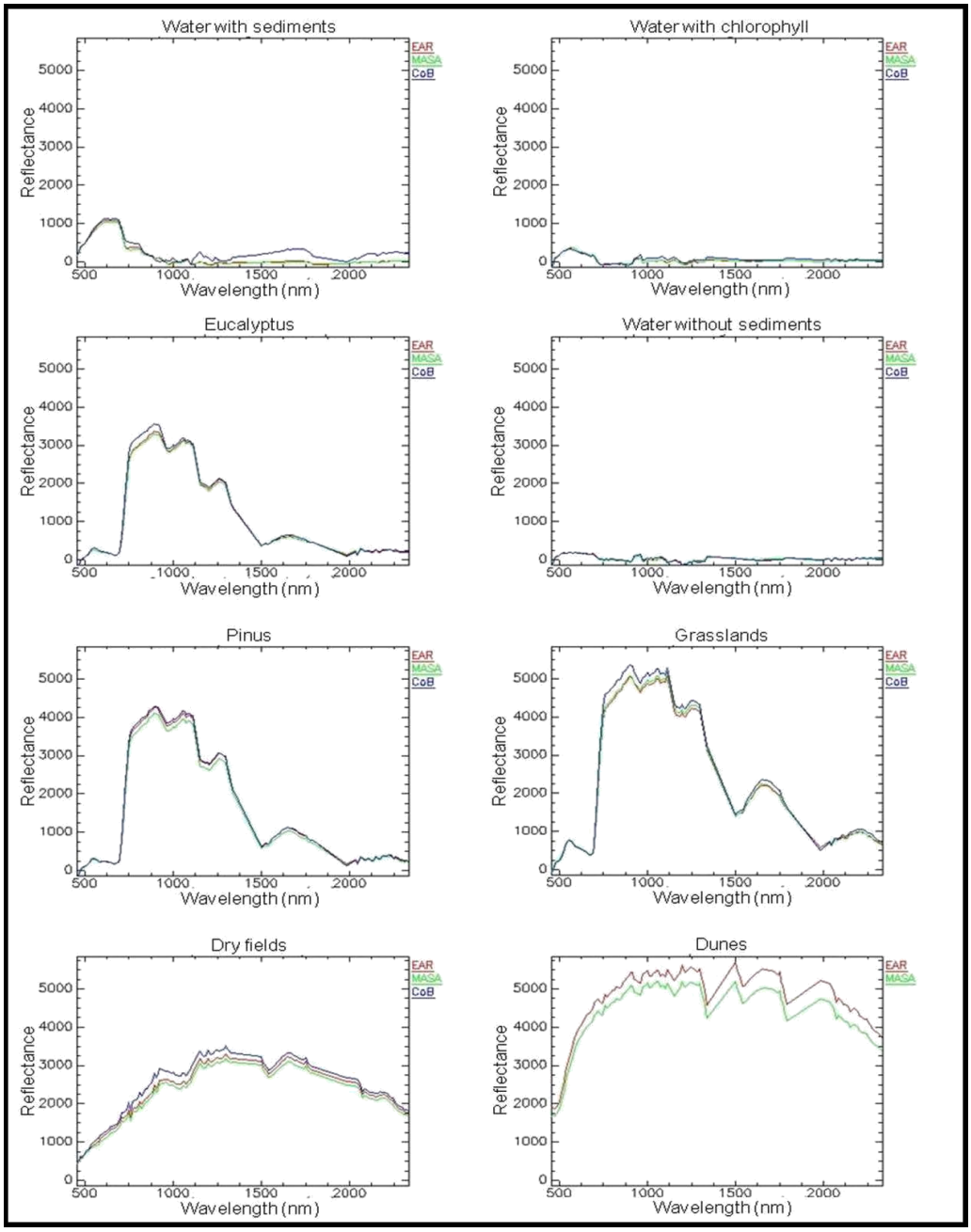

Figure 10: *Reflectance Spectra (X104) of Endmembers Selected By EAR, MASA and Cob Metrics to Build the Spectral Library. Data Around 1400 and 1900 nm Have No Significance Due to the Strong Atmospheric Absorption by Water Vapor*

3.2. MESMA Models

Results of the performance of two-, three-, and four-endmember models (see Table 3) are shown in Table 4. Although the subclasses water with sediment, grasses, and eucalyptus have been modeled with approximate values of 100 % for models with two and three endmembers, models with four endmembers had the smallest RMSE and a higher fraction for the five remaining subclasses.

Table 3: *Number of MESMA Models Generated by using the 2nd Spectral Library for Performance Evaluation*

Number of Endmembers	1st Endmember	2nd Endmember	3rd Endmember	4th Endmember	Number of Models
2	water/vegetation/soil	shade	-	-	23
3	water/soil	vegetation	shade	-	126
4	soil	vegetation	water	shade	405

Table 4: *Result Obtained from Two-, Three- and Four-Endmember MESMA Models (Endmembers) Applied to the Validation Sample. Values in Blue Refer to the Lowest RMSE; Values in Red Refer to Fractions Nearest to 100 %*

Subclasses	2 Endmembers		3 Endmembers		4 Endmembers	
	Fraction	RMSE	Fraction	RMSE	Fraction	RMSE
Water with Sediments	1,02217	0,00223	1,02841	0,00181	1,03081	0,00149
Water without Sediments	0,91303	0,00266	0,89781	0,00216	0,93011	0,00186
Water with Chlorophyll	0,88428	0,0022	0,88503	0,00182	0,89634	0,00144
Dry Fields	0,90515	0,01973	0,79719	0,00477	0,80143	0,00415
Dunes	0,95379	0,01555	0,93474	0,01387	0,96329	0,00493
Pinus	0,91926	0,00526	0,92953	0,00357	0,93104	0,00327
Eucalyptus	0,99622	0,00285	0,99648	0,00219	0,99593	0,00191
Grasslands	0,99479	0,00808	0,97786	0,0045	0,97538	0,00329
Average	0,94859	0,00732	0,93088	0,00434	0,94054	0,00279

Four endmember MESMA models were generated by attributing spectra of class soil (dune and dry field) spectra to the first component, spectra of class vegetation (pinus, eucalyptus and grasses) to the second component, and spectra of class water (water with sediment, water without sediment, and water with chlorophyll) to the third component.

After establishing the criteria, approximately 85 % of the Hyperion image was modeled by MESMA, which corresponds to 195,725 pixels (of a total of 230,400 pixels). Most pixels of the subclasses water, dry field, pinus, grasses, and eucalyptus were modeled and correctly classified. Only 46.25 % of the subclass dunes sample was modeled (see Table 5).

Table 5: *Results Obtained by Applying a Four-Endmember MESMA Model to the Validation Sample.*

Classes	Subclasses	% Modeled
Water	Water with Sediments	100,00%
	Water without Sediments	100,00%
	Water with Chlorophyll	100,00%
Vegetation	Pinus	100,00%
	Eucalyptus	100,00%
	Grasslands	97,50%
Soil	Dry Fields	100,00%
	Dunes	46,25%

The fraction images in Figure 11 show that the classes soil and vegetation, plus the endmember shade, were used together to model their respective areas, with the exception of sites with a more homogeneous cover of pinus, eucalyptus, grasses, dunes and dry field (attested by the high value of

brightness in the soil and vegetation fraction images). Pixels corresponding to the class water (water with chlorophyll, water with sediment, and water without sediment) were mostly modeled by their corresponding endmembers, plus shade, in some cases being modeled by approximately 70 % of shade (Figure 12).

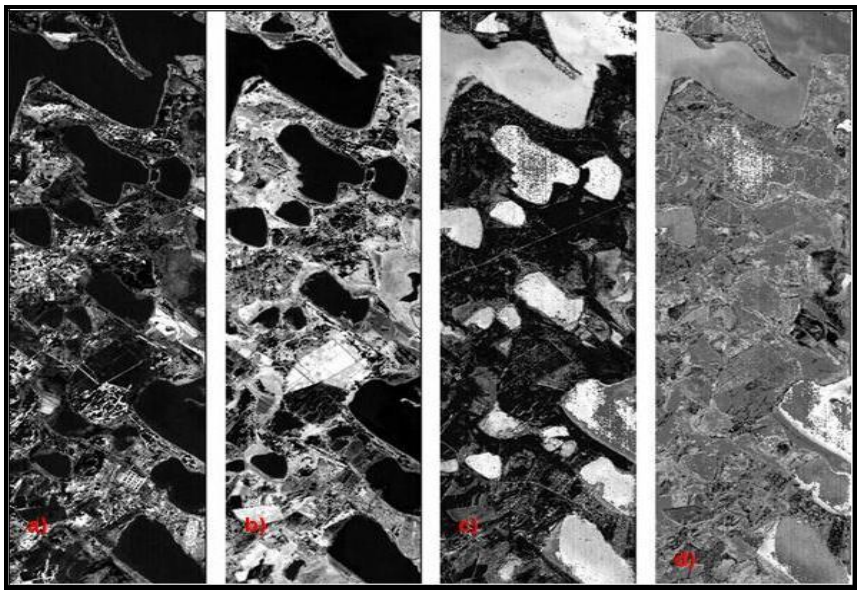

Figure 11: *Fraction Images Produced by VIPER Tools for Each Component of the MESMA Model: (a) Image, (b) Vegetation, (c) Water, and (d) Shade*

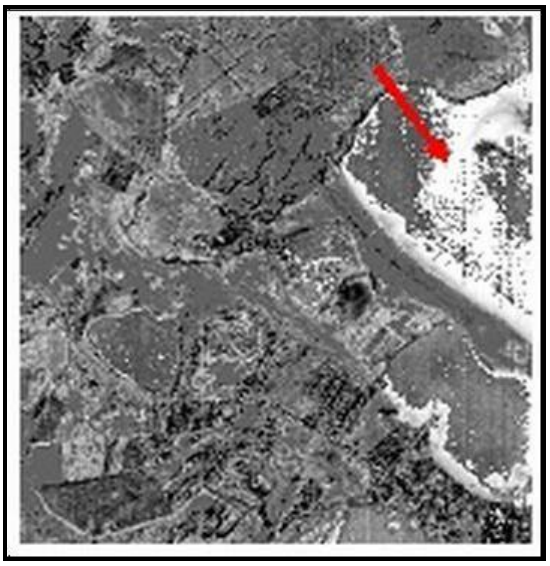

Figure 12: *Shade Fraction Image of a Portion of the Scene, Showing Pixels of Water with Sediment Modeled with a High Fraction of Shade (approx. 70 %)*

The RMSE image (Figure 13(a)) showed that the major errors resulted from MESMA when modeling grasses and dunes pixels, due to the high spectral variability of these targets. Spatial representation of variations in the fractions soil, vegetation and water is shown in Figure 13(b). It can be seen that those portions of most highlighted image (higher brightness) correspond to areas of greater abundance of one type of cover, e.g. those of pinus, eucalyptus and rice cultivation. The same was reported for water bodies and dry fields. Areas covered by other materials (e.g. grasses) showed signs of higher spectral mixture.

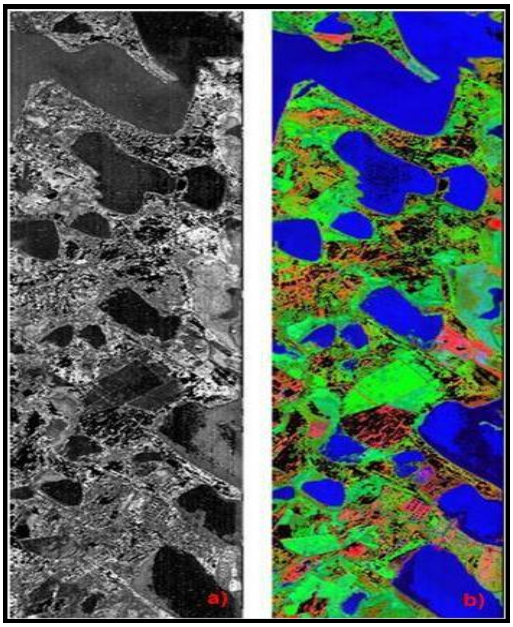

Figure 13: *(a) RMSE Image; (b) Color Composition of the Soil (Red), Vegetation (Green), and Water (Blue) Fractions. Black Areas in (b) were not modeled*

Figure 14 shows the fraction interval produced by MESMA for the eight subclasses studied herein. With the histogram of each image, it was observed that most pixels of the class water were modeled with fractions higher than 90 %. In the class vegetation, the mean fractions varied between 60 % (grasses) and 90 % (pinus and eucalyptus). The class soil showed the lowest fraction values, with approximately 50 % for the subclasses dry field. Subclass dunes showed an almost linear distribution, with an interval of 20 104 %.

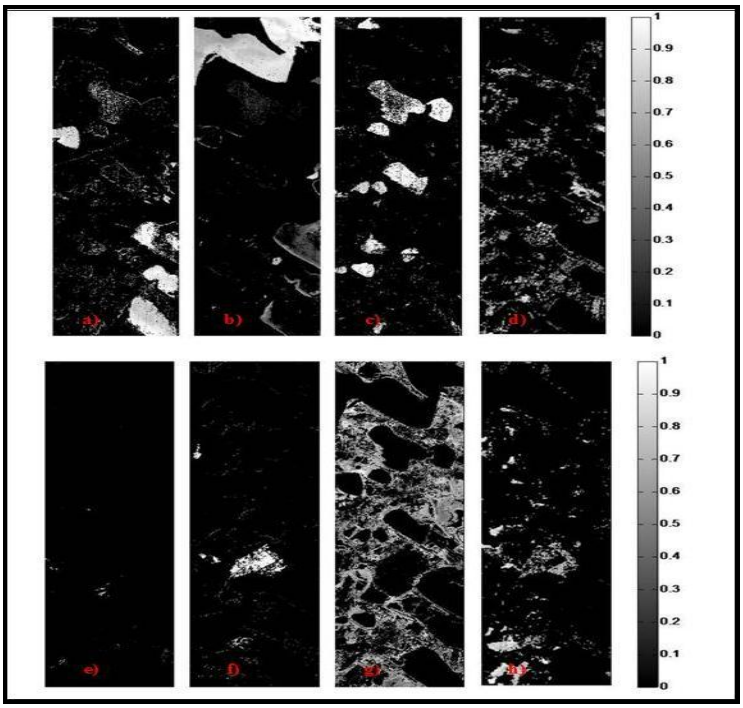

Figure 14: *Fraction Images of the Eight Subclasses: (a) Water with Chlorophyll, (b) Water with Sediment, (c) Water without Sediment, (d) Dry Field, (e) Dunes, (f) Eucalyptus, (g) Grasses, and (h) Pinus*

The final classification (Figure 15), obtained from images of the fractions soil, vegetation and water, show the spatial distribution of the eight subclasses studied herein. The analysis of the square array images shows that some areas corresponding to eucalyptus plantations had been classified as pinus; however, the opposite was not true. For the class water, results seem to be consistent with the true color image in Figure 2.

However, in the shallower sites (margins), there was a slight confusion between subclasses water with sediment and water with chlorophyll, mainly due to bottom effects. Just as with the validation samples, most areas covered with dunes were not modeled. The urban area, which was not represented in the mixture models, was modeled in part as dry field (soil). Figure 16 shows results obtained by MESMA when modeling part of the urban area of Tramandaí, located at the right lower corner of the Hyperion image.

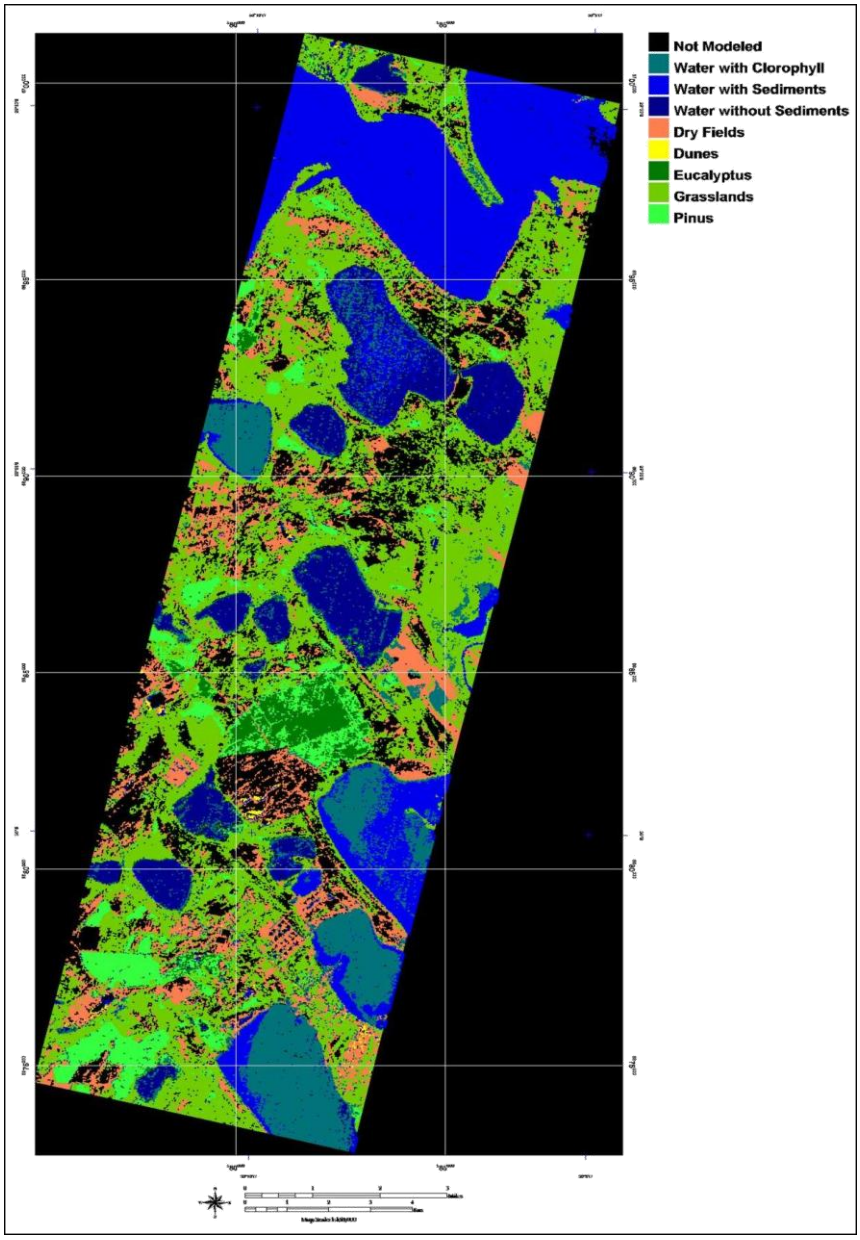

Figure 15: *Results Obtained by Using the Four-Endmember MESMA Model. Image was Classified Based on the Endmember with the Highest Fraction*

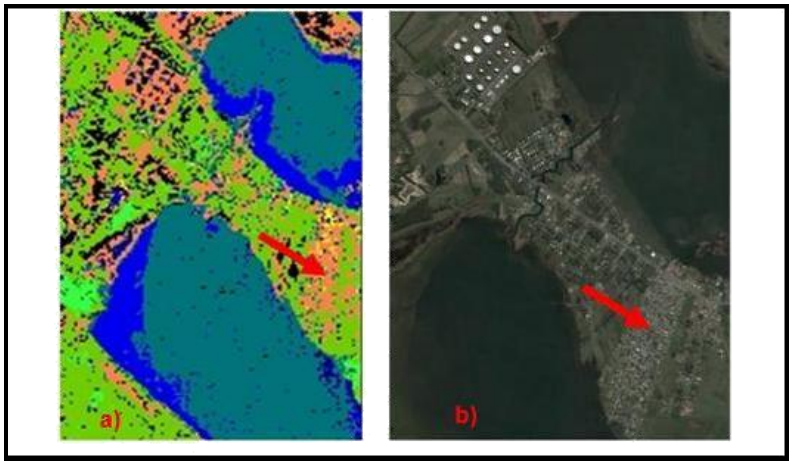

Figure 16: *Results Obtained by MESMA over Part of the Urban Area of Tramandaí: (a) Classified Image. Reddish Areas were classified as Dry Field (Soil); (b) Quickbird Image over Urban Area*

4. Conclusions

The final selection of endmembers to produce MESMA models can be done by using EAR, MASA and CoB metrics implemented with VIPER Tools software, which, when used together, are less sensitive to the effects of a low signal-to-noise ratio of the Hyperion sensor; When applied to the image and to the validation sample, the four-endmember MESMA model (soil = dunes and dry field; green vegetation = pinus, eucalyptus, and grasses; water = with suspended sediments, without sediments, and with chlorophyll; shade) appropriately described the diversity of the components of the scene, including materials within a same class (e.g. pinus and eucalyptus);

The application of the MESMA model to Hyperion data allowed satisfactorily identifying and quantifying materials constituting the area of study, except for a slight intra-class confusion, whereby endmembers of the subclass pinus modeled some eucalyptus pixels. When modeling "pure" pixels, fractions produced by the MESMA models met the expected values, largely achieving fractions higher than 90 %, with low RMSE;

The VIPER Tools software, with its friendly and easy-to-use interface, showed to be an efficient tool to select the most representative endmembers of each subclass and to apply MESMA models;

For endmembers derived from their own image, it is essential to have prior knowledge of the classes to be represented, since the user will have to attribute them to the spectra in the metadata file;

EAR, MASA and CoB metrics were implemented to help identifying the most representative endmembers i.e., those that best modeled their own classes. However, for an accurate quantitative analysis of the fractions generated, it is necessary to apply "pure" endmembers.

Results, on a whole, show the potential of using MESMA models with hyperspectral data from the Hyperion/EO-1 sensor, even considering the low signal-to-noise ratio of this tool, particularly in the SWIR. New paragraph: use this style when you need to begin a new paragraph.

Acknowledgements

The authors are grateful to CAPES (Coordenação de Aperfeiçoamento de Pessoal de Nível Superior), and to all anonymous reviewers for their very useful comments.

References

[1] Pearlman, J., Seagal, C., Liao, L., Carman, S., Folkman, M., Browe, B., Ong, L. and Ungar, S. 2000: *Development and Operations of the EO-1 Hyperion Imaging Spectrometer*. http://eo1.gsfc.nasa.gov/miscPages/TechForumOther/Yperion%20SPIE%20Publication.pdf (accessed Nov 24, 2006).

[2] Goodenough, D.G., Bhogal, A.S., Dyk, A., Hollinger, A., Mah, Z., Niemann, K.O., Pearlman, J., Chen, H., Tan, T., Love, J. and Mcdonald, S. *Monitoring Forest with Hyperion and ALI.* IEEE Transactions on Geoscience and Remote Sensing. 2002. 2; 882-885.

[3] Galvão, L.S., Formaggio, A.R. and Tisot, D.A. *Discrimination of Sugarcane Varieties in Southeastern Brazil with EO-1 Hyperion data.* Remote Sensing of Environment. 2005. 94; 523-534.

[4] Shimabukuro, Y.E. and Smith, J.A. *The Least-Squares Mixing Models to Generate Fraction Images Derived from Remote Sensing Multispectral Data.* IEEE Transactions on Geoscience and Remote Sensing. 1991. 29; 16-20.

[5] Smith, P.S., Balonek, T.J., Heckert, P.A., Elston, R. and Schmidt, G.D. *UBVRI Field Comparison Stars for Selected Active Quasars and BL Lacertae Objects.* Astronomical Journal. 1985. 90; 1184-1187.

[6] Roberts, D.A., Gardner, M., Church, R., Ustin, S., Scheer, G. and Green, R.O. *Mapping Chaparral in the Santa Monica Mountains using Multiple Endmember Spectral Mixture Models.* Remote Sensing of Environment. 1998. 65; 267-279.

[7] Dennison, P.E. and Roberts, D.A. *Endmember Selection for Multiple Endmember Spectral Mixture Analysis Using Endmember Average RMSE.* Remote Sensing of Environment. 2003. 87; 123-135.

[8] Dennison, P.E., Halligan, K.Q. and Roberts, D.A. *A Comparison of Error Metrics and Constraints for Multiple Endmember Spectral Mixture Analysis and Spectral Angle Mapper.* Remote Sensing of Environment. 2004. 93; 359-367.

[9] Roberts, D.A., Keller, M. and Soares, J.V. *Studies of Land-Cover, Land-Use, and Biophysical Properties of Vegetation in Large Scale Biosphere Atmosphere experiment in Amazonia.* Remote Sensing of Environment. 2003. 87; 377-388.

[10] Roberts, D.A., Halligan, K. and Dennison, P. 2007: VIPER Tools User Manual. Version 1.2. http://www.vipertools.org (accessed April 18, 2007).

[11] Matlab, Version 7.2; *Software for Numerical Computation, Visualization, and Programming*; Math Works: Massachusetts, U.S.A. 1984.

[12] Linn, R.M.; Rolim, S.B.A., and Galvão, L.S. *Assessment of the Multiple Endmember Spectral Mixture Analysis (MESMA) Model applied to the Hyperion/EO-1 Hyperspectral data of the Coastal plain of Rio Grande do Sul, Brazil.* ISPRS 100 Years, Vienna, Austria, July 5-7, 2010, IAPRS, Vol. XXXVIII, Part 7A; 134-138.